Journal of Molecular Liquids 417 (2025) 126673

Contents lists available at ScienceDirect

Journal of Molecular Liquids

journal homepage: www.elsevier.com/locate/molliq

Phase diagram and structure of TIP4P/2005 water and magnesium perchlorate: A molecular dynamic study of Martian aqueous solutions

Paolo La Francesca, Paola Gallo *

Dipartimento di Matematica e Fisica, Università degli studi Roma Tre, via della Vasca Navale 84, Roma, 00146, Italy

ARTICLE INFO

Keywords:
Molecular dynamics
Supercooled aqueous solutions
Magnesium perchlorate

ABSTRACT

We investigate the phase diagram and the structural behaviour of magnesium perchlorate solutions in supercooled TIP4P/2005 water via molecular dynamics numerical simulations for solute concentrations of 2.95 wt% (mole fraction 2.45×10^{-3}) and 24.4 wt% (mole fraction 25.4×10^{-3}). These solutions hold particular significance due to recent experimental findings about the presence of liquid water in perchlorate solutions underneath the Martian surface. Upon increasing the concentration of the solutes, an interplay between the high-density liquid (HDL) and the low-density liquid (LDL) phases of water is found. Similar to the pure phase of water, at low concentration the system shows a liquid-liquid critical point. No liquid-liquid critical point was found for the higher concentration. Nonetheless, several water anomalies persist in both solutions. We observe that the LDL region shrinks as the concentration is increased. The structural analysis confirms the interplay between HDL and LDL, albeit HDL local structure prevails in the solutions more than in pure water.

1. Introduction

One of the most fascinating topics in statistical mechanics and condensed matter physics is the study of the structural and thermodynamic behaviour of water. Water, indeed, exhibits a significant number of anomalies, whose origin is still not entirely clear [1–6].

Such anomalies are even more striking when water is supercooled, i.e. kept liquid below its freezing temperature. Molecular Dynamics (MD) simulations on the ST2 model for water [7] led, in 1992, to the formulation of the hypothesis of the existence of a second-order liquid-liquid critical point (LLCP) in the supercooled region of water [8]. Under this hypothesis, at temperatures below the critical point, water exists in two separate phases: high-density liquid (HDL) and low-density liquid (LDL).

Simulations have rigorously shown that the LLCP exists in the ST2 model for water [9–14], Jagla [15] as per [16], and TIP4P/2005 [17] and TIP4P/Ice [18] as per [19]. An experimental proof of the hypothesis is particularly challenging because of nucleation. Nonetheless, its existence has been indirectly shown in several experiments [20–24].

While no impediment prevents liquid water to reach the glassy state through supercooling [25], the presence of impurities favours the nucleation process that occurs naturally in systems undergoing a first-order transition (such as the liquid-to-ice transition). The LLCP is estimated to be located in a region referred to as the “no man’s land”, where nucleation occurs so rapidly for water that experiments cannot access it. Recently, however, the experimental borders of the no man’s land have been shrunk [21,26,27].

Because of their fast cooling rates, simulations make it possible to explore the entire phase diagram of supercooled water, hence playing a key role in investigating supercooled regions not experimentally accessible [28,6].

Through MD simulations, a singular Ising-like behaviour for the LLCP was proven to occur at $T_C = 172$ K and $p_C = 186$ MPa for the TIP4P/2005 [19], which together with the TIP4P/Ice is one of the most realistic water models currently available to reproduce the phase diagram of water.

The theory of critical phenomena predicts that when a second-order critical point is approached from the single-phase region, a line of correlation length maxima emerges, the Widom Line. Both simulations and experiments have proven its existence in the supercooled region of water’s phase diagram, providing further evidence for the existence of the LLCP [29–33,21,34]. We note that this line has also been proven to be clearly detectable in water above the well-known liquid-gas critical point in experiments and simulations [35].

The research of water anomalies is inherently interconnected to that of supercooled aqueous solutions, as water is not only typically found in solutions, but is often easier to supercool in them [36–39].

More to the point of aqueous solutions, we have recently used MD simulations to show that the LLCP persists at least for concentrations

* Corresponding author.
E-mail address: paola.gallo@uniroma3.it (P. Gallo).

https://doi.org/10.1016/j.molliq.2024.126673
Received 22 July 2024; Received in revised form 6 November 2024; Accepted 1 December 2024

Available online 5 December 2024

Table 1
Number of ions and water molecules of the two systems investigated and the corresponding concentrations reported both in weight percentage and in mole fraction.

$N_{Mg^{2+}}$	$N_{ClO_4^-}$	N_{H_2O}	Conc. (wt%)	Conc. (mole frac. $\times 10^{-3}$)
10	20	4072	2.95	2.45
100	200	3838	24.4	25.4

from low to moderate and shifts to higher temperatures and lower pressures upon increasing the concentration of the solute when considering aqueous solutions of sodium perchlorate [40]. Furthermore, in the same study, we have shown that water anomalies, like the Temperature of Maximum Density (TMD) line, the Temperature of Minimum Density (TmD) line and the Widom Line pointing to the LLCP, persist.

Aqueous solutions of perchlorates are highly topical, as they are believed to be the key to explaining the recent radar detection of subglacial liquid water on Mars [41,42].

In our previous study [40], the anomalous properties of water have been shown to play an important role. In particular, compared to the pure phase, aqueous (TIP4P/2005) $NaClO_4$ solutions were found to be stabilising the HDL region of water upon increasing the solute concentration by inducing a contraction of the LDL phase, where nucleation is favoured [1].

Experiments have shown that while aqueous solutions of sodium perchlorate can be supercooled down to 223 K, this temperature shifts to approximately 150 K for magnesium perchlorate ($Mg(ClO_4)_2$) [43]. Moreover, even at high concentrations, the hydrogen-bonded network of water is not completely disrupted by perchlorate ions, the effect of which on water is akin to a compression [44–46]. In dilute sodium perchlorate solutions water anomalies persist up to 2M [47].

In this paper, we show the results of MD simulations performed on aqueous solutions of $Mg(ClO_4)_2$, a salt that is significantly present on Mars.

The structure of the paper is the following: in section 2 we explain how we built the system, in section 3 the phase diagrams are reported, in section 4 we report the structural results, in section 5 we compare sodium and magnesium perchlorate solutions and in section 6 we present the conclusions.

2. Methods

MD simulations were carried out in the canonical ensemble using the GROMACS 5.1.4 software suite [49–51]. Two concentrations were considered, $C_1 = 2.95\,\text{wt\%}$ (mole fraction 2.45×10^{-3}) and $C_2 = 24.4\,\text{wt\%}$ (mole fraction 25.4×10^{-3}), obtained with the number of particles reported in Table 1.

Water was modelled using the TIP4P/2005 potential [17] and $Mg(ClO_4)_2$ using the potential defined in [52] with a Lennard-Jones cutoff radius of 0.95 nm and Lorentz-Berthelot combination rules. For the potential defined in [52], the Lennard-Jones parameters for Mg were derived from aqueous (SPC) ionic solution data in Ref. [53], and those for perchlorate were based on aqueous (ST2) solutions of sodium perchlorate [54]; the Lorentz-Berthelot mixing rules were then applied by Ref. [52]'s authors to determine the cross-interaction parameters.

The simulation time-step for the leapfrog algorithm was set to 1 fs [28]. Periodic boundary conditions were applied. Electrostatic interactions were considered using the Particle-Mesh Ewald method [55]. The v-rescale thermal coupling [56] was employed.

We simulated 27 isochores at concentration C_1, spanning from $880\,\text{kg/m}^3$ to $1140\,\text{kg/m}^3$, and 28 isochores at concentration C_2 spanning from $\rho = 970\,\text{kg/m}^3$ to $1200\,\text{kg/m}^3$. For each isochore, we simulated state points at temperatures ranging from 400 K to 170 K, while the simulation times were increased from 100 ps for the highest temperature to 40 ns for the lowest. The equilibration times were chosen by ensuring that at the conclusion of each run the state points were suitably equilibrated as the energy had reached its minimum value.

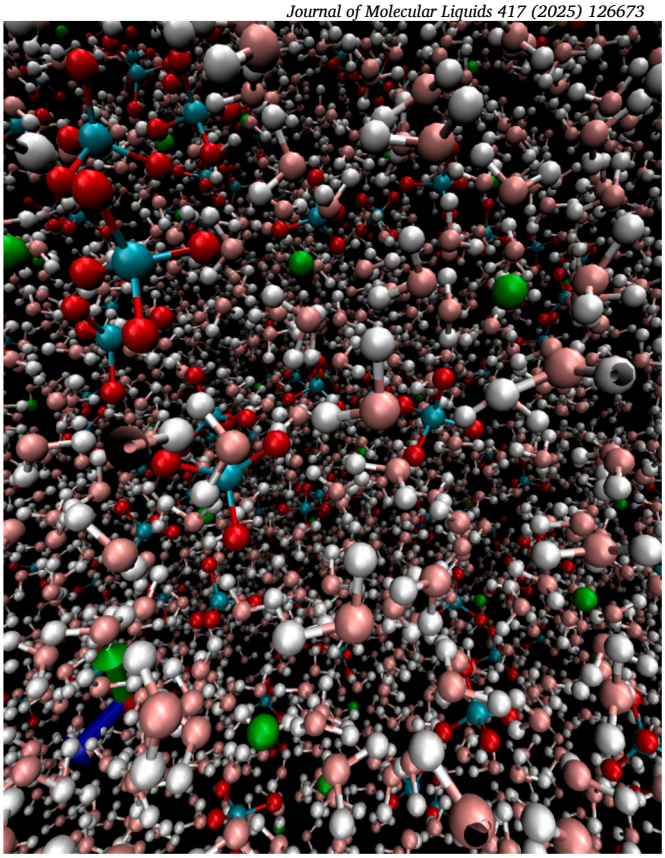

Fig. 1. Snapshot of a 24.4 wt% (mole fraction 25.4×10^{-3}) aqueous magnesium perchlorate solution at $\rho = 1200\,\text{kg/m}^3$ and $T = 200\,\text{K}$. The water molecule is shown in pink (oxygen) and grey (hydrogen), the magnesium ion in green, and the perchlorate ion in teal (chlorine) and red (oxygens). Created using VMD [48].

For each concentration, we progressively lowered the density until we reached the liquid-gas limit of mechanical stability (LG-LMS), which in our simulations was characterised by the occurrence of cavitation, with a consequent sudden increase of the pressure resulting from the formation of vapour bubbles [57]. A total number of 1455 state points was simulated.

A snapshot of the C_2 solution is presented in Fig. 1 which, upon visual inspection, shows that the ions are well mixed with the water.

3. Phase diagrams

In this section, we report the thermodynamic results of our simulations.

3.1. Findings for the C_1 solution

In Fig. 2 we report all the isochores calculated for the C_1 solution, covering densities ranging from $880\,\text{kg/m}^3$ to $1140\,\text{kg/m}^3$. Each line corresponds to an isochore.

In the figure, we can locate the region of density anomaly, which is undoubtedly the most well-known among the water anomalies. When water undergoes isobaric cooling, it exhibits a TMD. Below this temperature, it expands down to a TmD, restoring upon further cooling the normal simple liquid behaviour [58–60].

From the following relation

$$\left.\frac{\partial \rho}{\partial T}\right|_p = -\left.\frac{\partial p}{\partial \rho}\right|_T^{-1} \left.\frac{\partial p}{\partial T}\right|_\rho \tag{1}$$

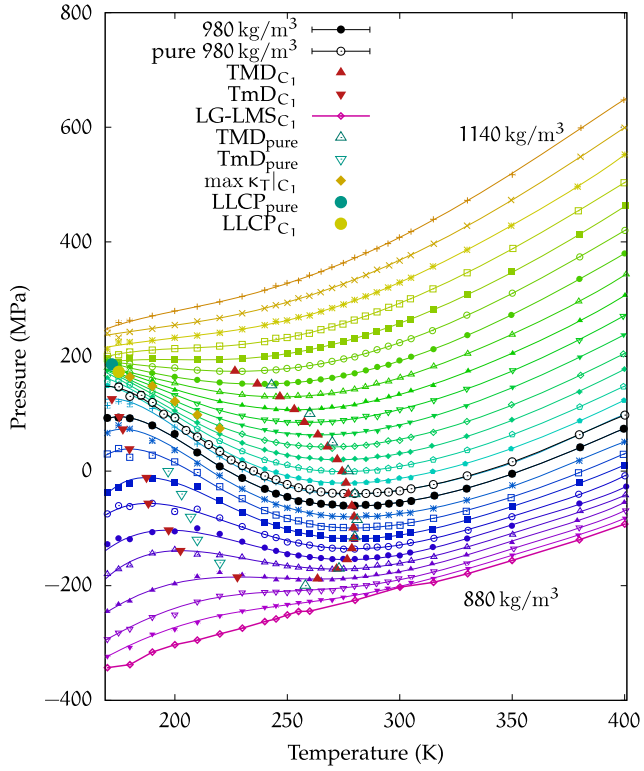

Fig. 2. Equation of state for the C_1 solution. Isochores at densities ranging from $\rho = 1140\,\mathrm{kg/m^3}$ to $\rho = 880\,\mathrm{kg/m^3}$ with increments $\Delta\rho = 10\,\mathrm{kg/m^3}$ are plotted in the (p,T) plane for temperatures from $T = 400\,\mathrm{K}$ to $170\,\mathrm{K}$. Symbols represent the state points obtained from the simulations and the lines are polynomial fits to the simulated state points. The TMD curves for the solution are depicted using red-filled triangles up, whereas the empty teal ones correspond to pure TIP4P/2005. The convergence of the isochores, in conjunction with the flattening of the curves in Fig. 3, as well as the highest peak in Fig. 4, provides an estimated position of the LLCP at $T_C = 175\,\mathrm{K}$ and $p_C = 173\,\mathrm{MPa}$ (yellow circle). The pure TIP4P/2005 LLCP [19] is symbolised by a teal-filled circle and the Widom line of the C_1 solution is represented by dark yellow filled diamonds. The LG-LMS $880\,\mathrm{kg/m^3}$ isochore is the thick magenta line at the bottom. Additionally, the $980\,\mathrm{kg/m^3}$ isochores for the C_1 solution (black-filled circles) and the pure phase (black empty circles) are highlighted.

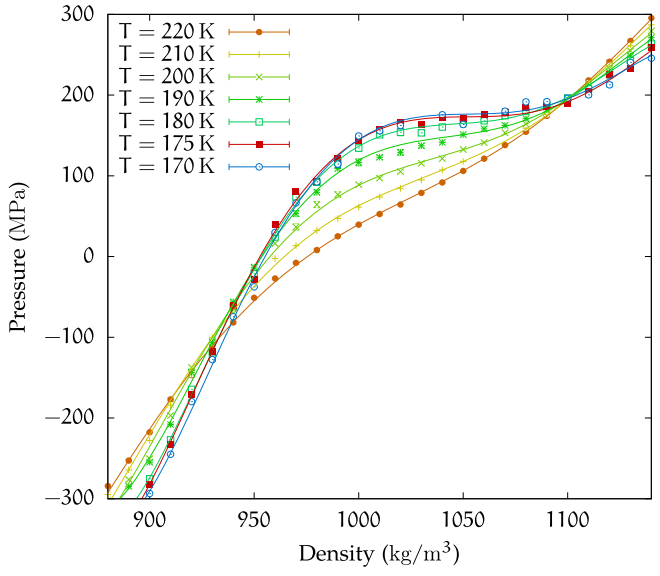

Fig. 3. Equation of state for the C_1 solution plotted in the isotherm plane. The 175 K isotherm curve can be seen flattening at $1052\,\mathrm{kg/m^3}$ and 173 MPa.

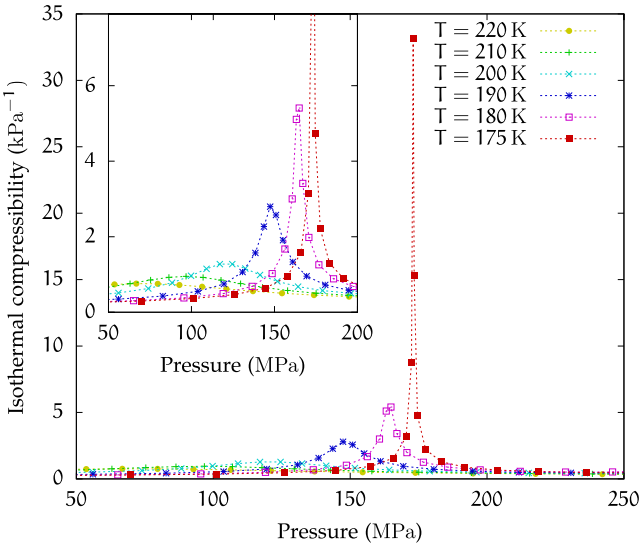

Fig. 4. Isothermal compressibility for the C_1 solution.

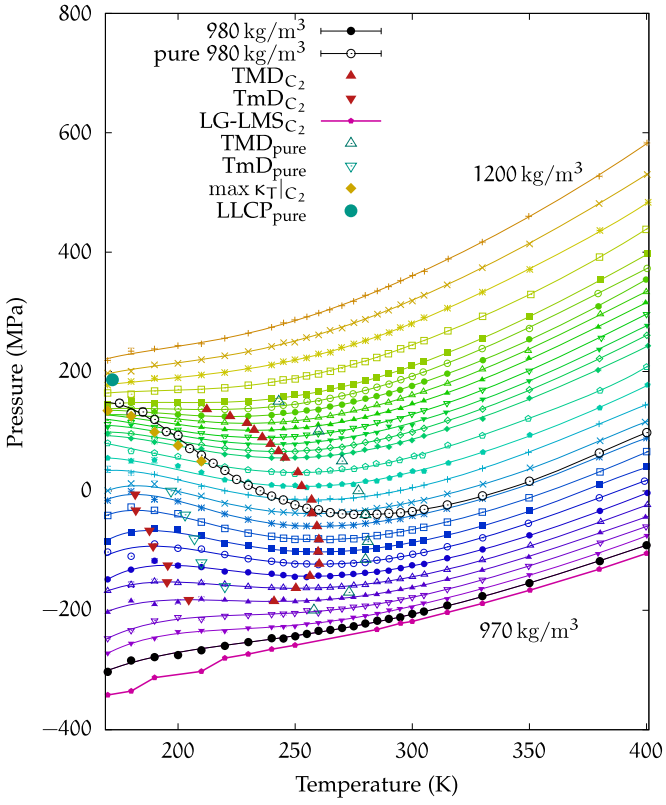

Fig. 5. Equation of state for the C_2 solution. In the (p,T) plane we plot isochores at densities ranging from $\rho = 1200\,\mathrm{kg/m^3}$ to $\rho = 970\,\mathrm{kg/m^3}$ with increments $\Delta\rho = 5\,\mathrm{kg/m^3}$ in the range $[1120\,\mathrm{kg/m^3}, 1160\,\mathrm{kg/m^3}]$ and $\Delta\rho = 10\,\mathrm{kg/m^3}$ elsewhere, for temperatures from $T = 400\,\mathrm{K}$ to $170\,\mathrm{K}$. Symbols represent the state points obtained from the simulations and the lines are polynomial fits to the simulated state points. The TMD curves for the solution are depicted using red-filled triangles up, whereas the empty teal ones correspond to pure TIP4P/2005. No critical points were detected in the range of temperatures investigated. The pure TIP4P/2005 LLCP [19] is symbolised by a teal-filled circle and the isothermal compressibility maxima curve of the C_2 solution is represented by dark yellow filled diamonds. The LG-LMS $970\,\mathrm{kg/m^3}$ isochore is the thick magenta line at the bottom. Additionally, the $980\,\mathrm{kg/m^3}$ isochores for the C_2 solution (black-filled circles) and pure water (black empty circles) are highlighted.

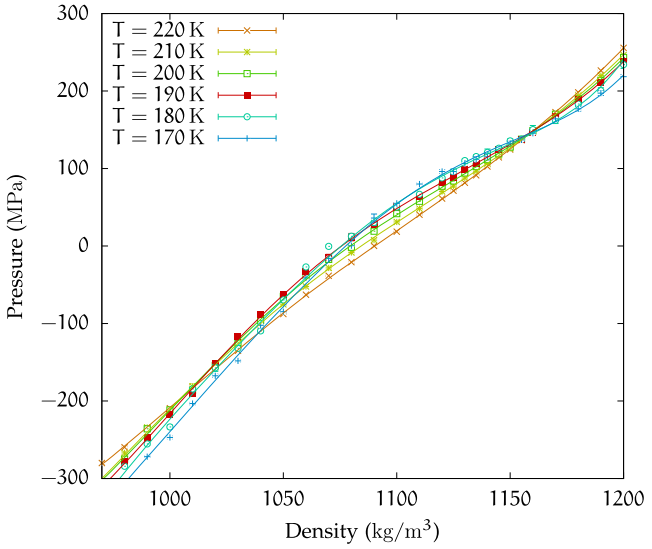

Fig. 6. The equation of state for the C_2 solution is plotted in the isotherm plane. Lines are polynomial fits to the simulated state points.

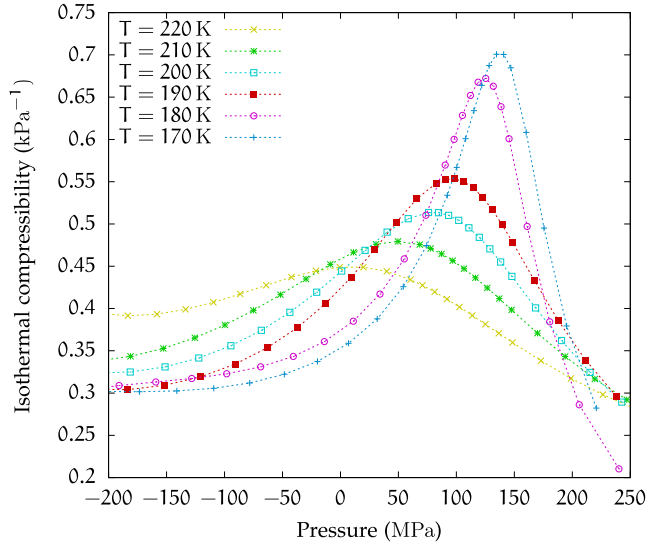

Fig. 7. Isothermal compressibility for the C_2 solution.

it results that the isochores' stationary points provide the location of the state points corresponding to the temperatures of density extrema.

In particular, from the isochores' minima, it is possible to determine the TMD curve, while the TmD curve can be similarly determined by their maxima.

We observe from Fig. 2 that both the TMD and TmD lines are still present in the C_1 solution and these lines are shown alongside the corresponding ones known for the pure phase in the literature [61].

We note that at this low concentration of $Mg(ClO_4)_2$, the TMD and the TmD of the C_1 solution appear to have shifted to lower temperatures and that the difference between the two curves is small.

In Fig. 2 we also display the isochore for the pure phase at 980 kg/m^3 which we calculated. This isochore is to be compared with the one at the same density for the C_1 solution here analysed. We can see that the 980 kg/m^3 isochore for the C_1 solution is slightly shifted to lower pressures.

The last isochore plotted in the figure corresponds to the LG-LMS, which was identified as described in Section 2. Below this line, the liquid mixture is mechanically unstable.

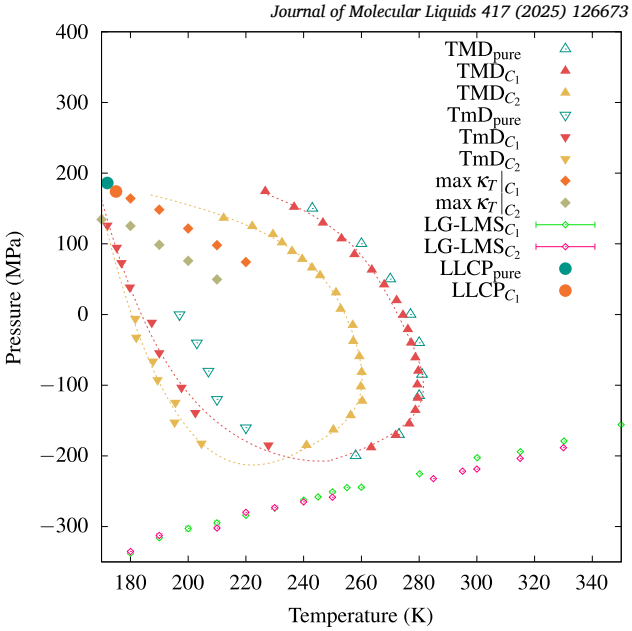

Fig. 8. Phase diagram for both the solutions without the isochores.

A second-order critical point between two condensed phases is characterised (see ref. [6]) by the condition

$$\left.\frac{\partial p}{\partial \rho}\right|_{T_C} = 0\,, \tag{2}$$

indicating the presence of an inflexion point with a horizontal tangent in the isotherm plane, which will be investigated here below.

Within the (p,T) plane, instead, when considering a discrete set of isochores, the Eq. (2) leads to

$$\frac{p(T_C,\rho)}{\Delta\rho} = \frac{p(T_C,\rho+\Delta\rho)}{\Delta\rho}\,, \tag{3}$$

implying that the critical region is located at the crossing of the isochores occurring at the highest temperature within the region of density anomaly.

In the (p,T) plane of the phase diagram that we show in Fig. 2, the isochore curves can be seen converging and the corresponding state points mark our estimate for the location of the critical region at approximately $T \approx 175$ K and $\rho \approx 1050$ kg/m^3.

This estimate is confirmed, in the (p,ρ) plane (Fig. 3), by the horizontal flattening of the isotherms around the inflexion point that at $T = 175$ K occurs at $\rho = 1052$ kg/m^3.

In order to provide an estimate of the Widom Line and to improve our understanding of the critical behaviour, it is possible to analyse the isothermal compressibility

$$\kappa_T = -\frac{1}{V}\left.\frac{\partial V}{\partial p}\right|_T \tag{4}$$

as a function of the pressures at the simulated state points.

We report the κ_T curves calculated from our simulations in Fig. 4. We see from Fig. 4 that κ_T has the typical behaviour expected for a critical phenomenon with the peak intensity strongly increasing at the critical point, confirming that the LLCP is also present in the C_1 solution.

The peaks of these curves provide a proxy for the location of the Widom Line [30]. The state points corresponding to the peaks are also reported in Fig. 2. The observed divergence of the 175 K peak indicates a critical pressure of $p_C^{(C_1)} = 173$ MPa.

On the basis of these results, we estimate the position of the LLCP for the C_1 solution at $T_C^{(C_1)} = 175$ K, $p_C^{(C_1)} = 173$ MPa and $\rho_C^{(C_1)} = 1052$ kg/m^3.

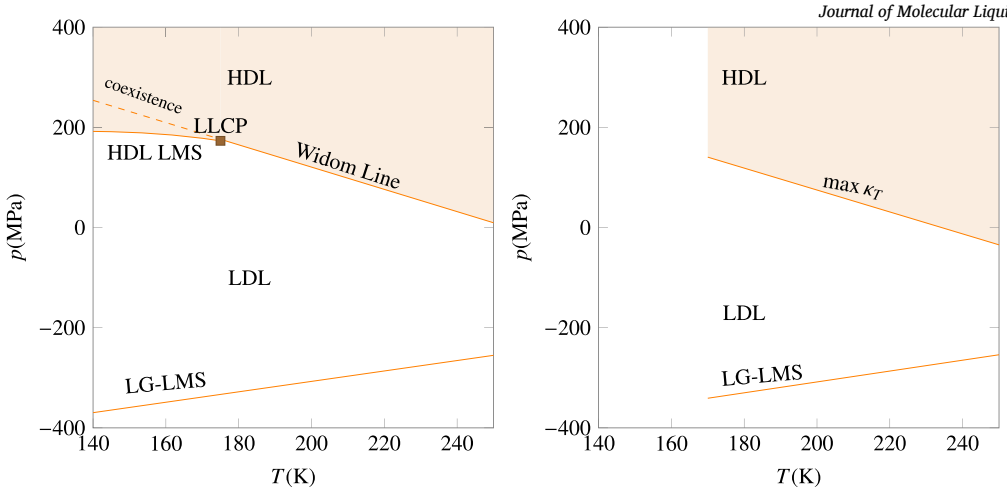

(a) C_1 = 2.95 wt% (mole fraction 2.45×10^{-3}) (b) C_2 = 24.4 wt% (mole fraction 25.4×10^{-3})

Fig. 9. Schematic phase diagrams for the two investigated solutions. The LDL region shrinks upon increasing the solute concentration.

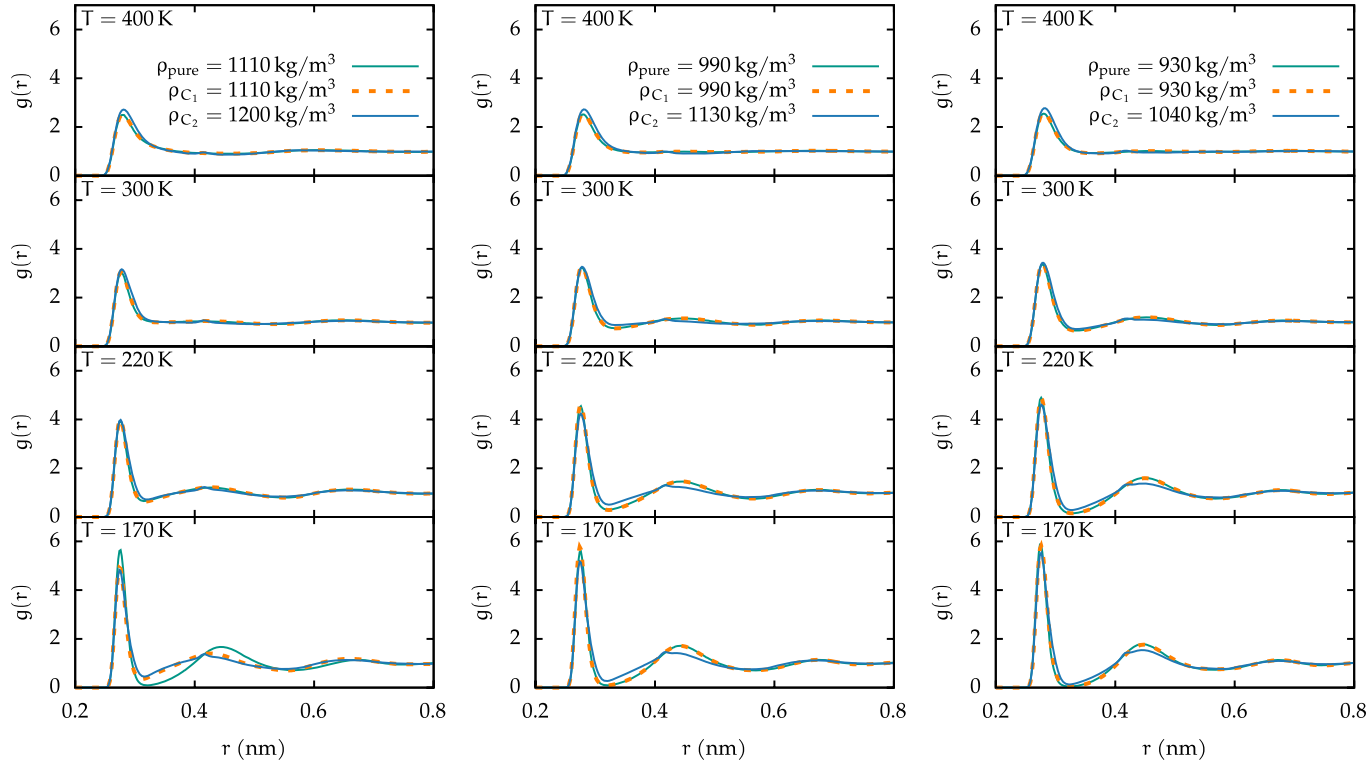

(a) $\rho_{\text{pure}} = \rho_{C_1} = 1110\,\text{kg/m}^3, \rho_{C_2} = 1200\,\text{kg/m}^3$ (b) $\rho_{\text{pure}} = \rho_{C_1} = 990\,\text{kg/m}^3, \rho_{C_2} = 1130\,\text{kg/m}^3$ (c) $\rho_{\text{pure}} = \rho_{C_1} = 930\,\text{kg/m}^3, \rho_{C_2} = 1040\,\text{kg/m}^3$

Fig. 10. Water-water ($O_W - O_W$) RDFs for pure water and for the C_1 and the C_2 solutions, corresponding to three sets of densities. The densities were chosen by matching isochore curves with similar pressures at low temperatures.

We report this point in Fig. 2. For reference, in the same figure we also report the pure TIP4P/2005 LLCP which was rigorously located at $T_C^{(\text{pure})} = 172\,\text{K}$ and $p_C^{(\text{pure})} = 186\,\text{MPa}$ by Debenedetti et al. in [19].

We note that in the C_1 solution the LLCP is shifted to a slightly lower pressure while the critical temperature is approximately the same.

3.2. Findings for the C_2 solution

We now discuss the thermodynamic results of the C_2 solution. All the isochores calculated for this system, with densities ranging from $970\,\text{kg/m}^3$ to $1200\,\text{kg/m}^3$ are plotted in Fig. 5.

For reference, the black-highlighted $980\,\text{kg/m}^3$ isochores for both pure TIP4P/2005 and the solution are plotted, a direct comparison between which shows for pure water a much more pronounced curvature than any of those plotted for the solution under investigation.

The TMD and TmD curves for the solution and pure TIP4P/2005 are also shown in Fig. 5. In particular, for the C_2 solution, these curves have shifted towards lower temperatures, while there has been no significant shift in terms of pressure.

The LG-LMS was identified, as discussed in the previous section, with the $970\,\text{kg/m}^3$ isochore. No significant shift in pressure of this line was observed with respect to the C_1-solution.

Looking at Fig. 5, we observe no evidence of crossing of isochores in the range of temperatures that could be investigated for the C_2 solution, although the $1145\,\text{kg/m}^3$ and the $1140\,\text{kg/m}^3$ curves appear to be very

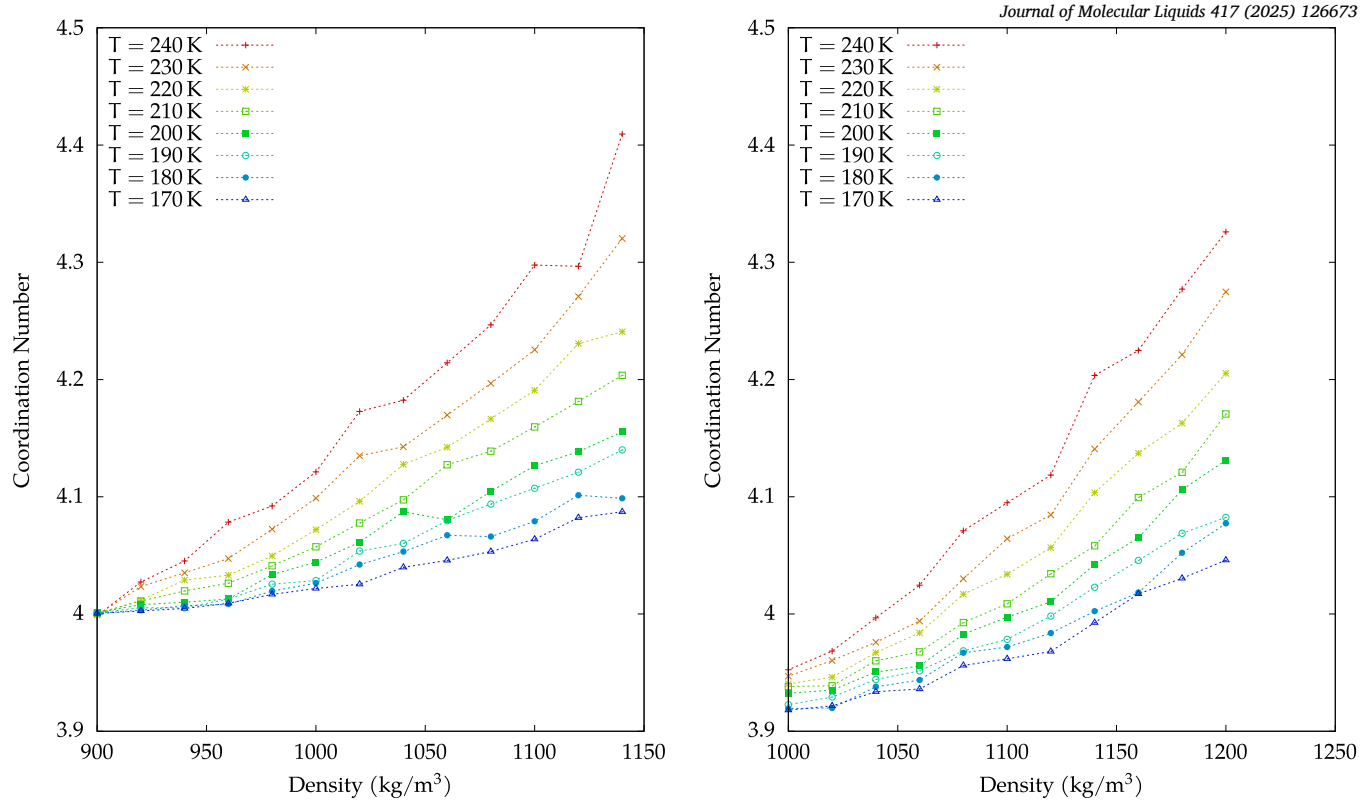

(a) C_1 = 2.95 wt% (mole fraction 2.45×10^{-3}) (b) C_2 = 24.4 wt% (mole fraction 25.4×10^{-3})

Fig. 11. $O_W - O_W$ first shell coordination numbers at constant temperatures as a function of density for the C_1 solution (panel (a)) and the C_2 solution (panel (b)).

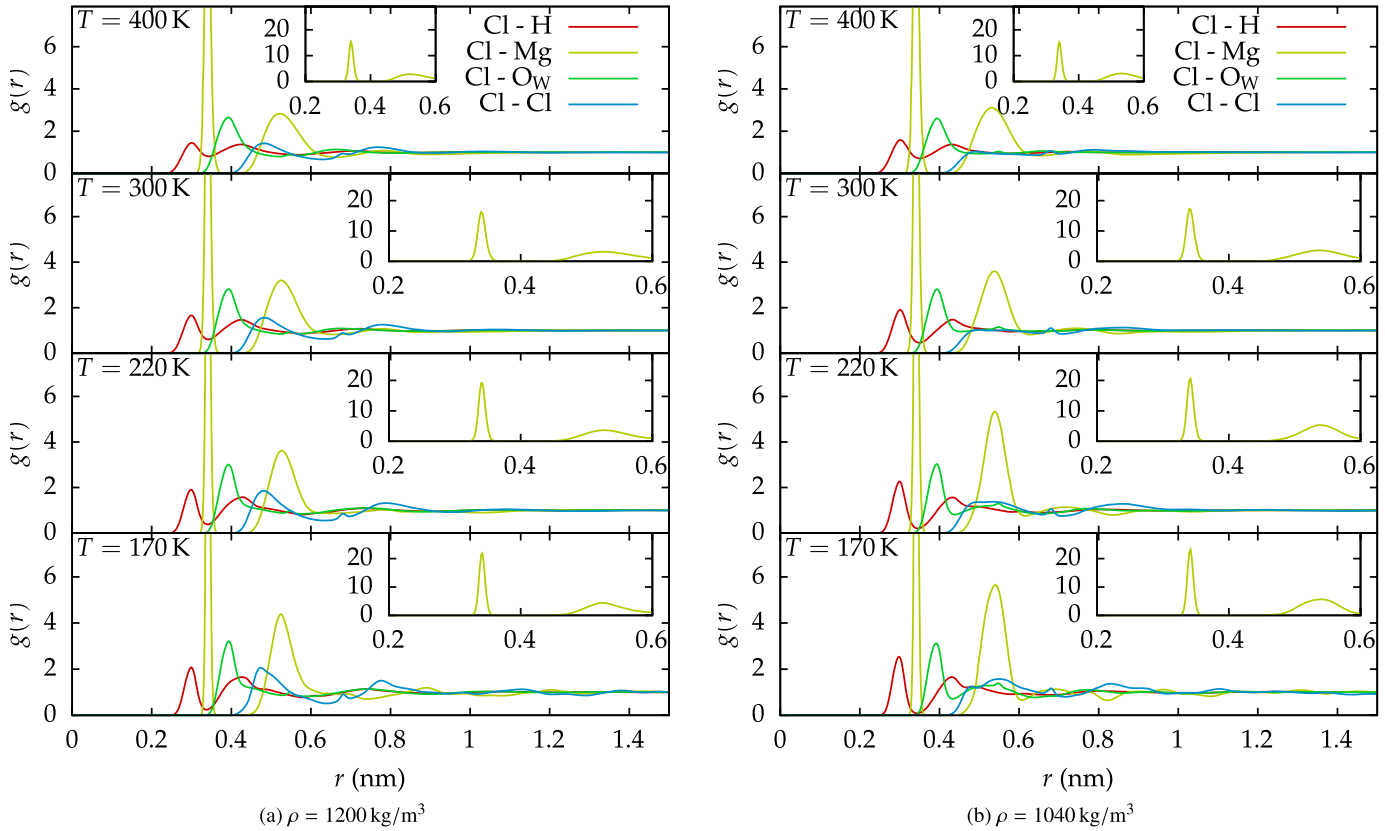

(a) ρ = 1200 kg/m^3 (b) ρ = 1040 kg/m^3

Fig. 12. Cl – H, Cl – Mg, Cl – O_W, Cl – Cl RDFs are presented for the C_2 solution at two different densities: (a) $\rho = 1200\,kg/m^3$ and (b) $\rho = 1040\,kg/m^3$. The graphs illustrate the coordination of chlorine by hydrogen, magnesium, oxygen, and chlorine in that order. The panels also specifically highlight the Cl–Mg RDF, displaying the height of the first peak on different scales.

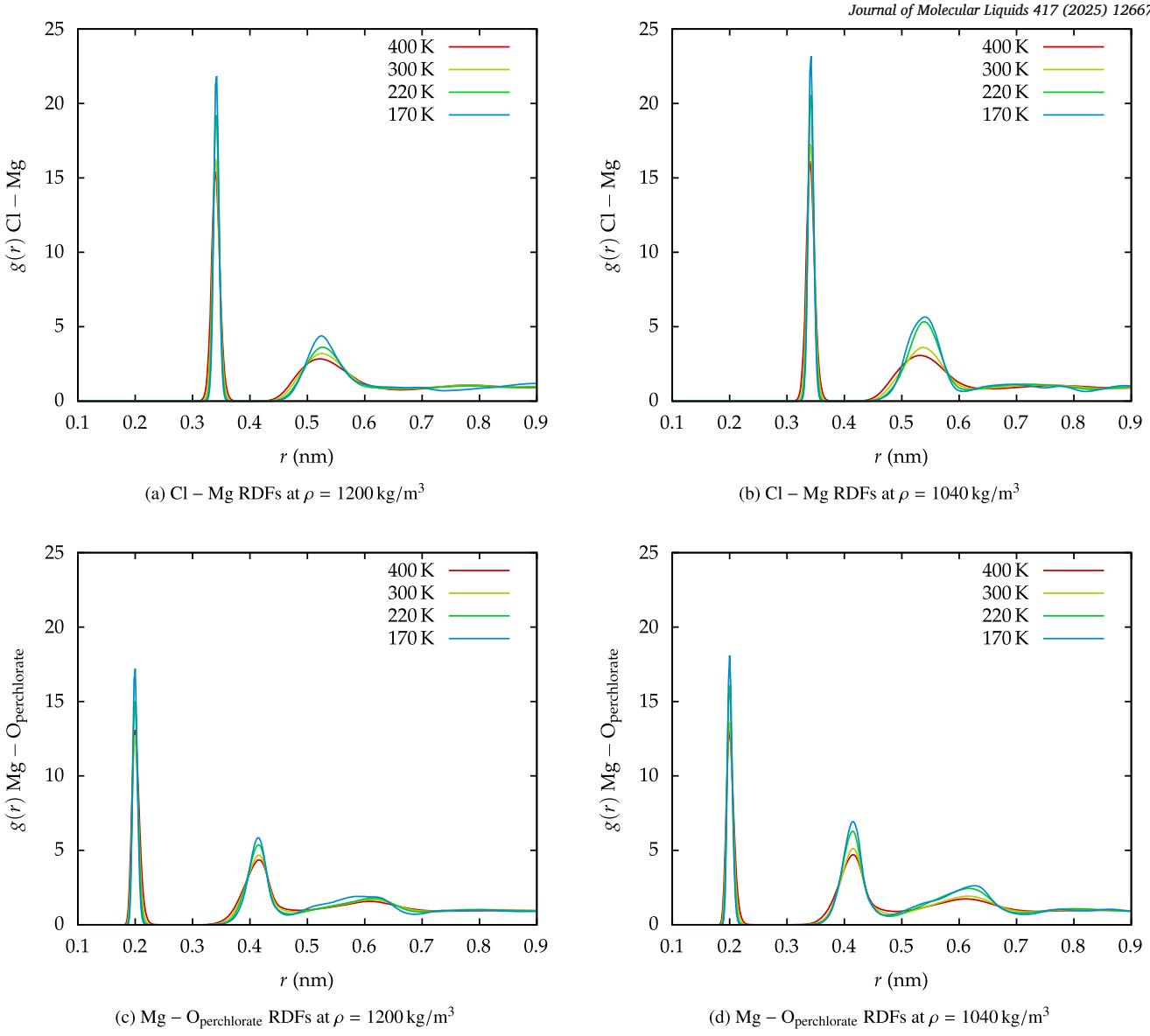

(a) Cl − Mg RDFs at $\rho = 1200\,\mathrm{kg/m^3}$

(b) Cl − Mg RDFs at $\rho = 1040\,\mathrm{kg/m^3}$

(c) Mg − $O_{perchlorate}$ RDFs at $\rho = 1200\,\mathrm{kg/m^3}$

(d) Mg − $O_{perchlorate}$ RDFs at $\rho = 1040\,\mathrm{kg/m^3}$

Fig. 13. Ion-Ion RDFs for the C_2 solution at densities $\rho = 1200\,\mathrm{kg/m^3}$ and $\rho = 1040\,\mathrm{kg/m^3}$.

close at the lowest temperature investigated, which was 170 K. In Fig. 5 we report for reference the position of the pure TIP4P/2005 LLCP [19].

To gain a better understanding of the system's behaviour at lower temperatures, the solution was investigated in the (p, ρ) plane reported in Fig. 6. At variance with the analogous results of the C_1 solution, we see no flattening of the curvature of the isotherms, which further reinforces the evidence of the absence of critical points in the regions of the phase diagram investigated.

However, the trend of the isothermal compressibility as a function of pressure highlighted in Fig. 7 shows an increase in the peaks with decreasing temperature. This trend, therefore, does not exclude the existence of an LLCP, which might possibly have shifted to lower temperatures, although the small increase of the isothermal compressiblity between 180 and 170 K seems to show that the anomalous behaviour has some residual characteristic but it is smeared out.

The state points corresponding to the κ_T peaks are also reported in Fig. 5.

3.3. Comparison

A comparison between the two phase diagrams is reported in Fig. 8 without the isochores. Upon increasing the concentration of the solute, the TMD curve shifts to lower temperatures, as does the TmD curve, albeit by a smaller amount. This translates into a shrunken region of density anomaly.

In the C_1 solution, the LLCP has a minor downward shift in pressure while the critical temperature is approximately the same. No critical points, instead, are evident in the region considered for the C_2 solution.

No significant displacement in pressure was observed in the LG-LMS.

The pressure of the isothermal compressibility peaks, which for the C_1 concentration also serve as a proxy for the Widom Line, decreased as the concentration increased.

The Widom Line separates the HDL-like region from the LDL-like region. Although no critical points (and therefore no Widom Line points) are observed in the C_2 solution, the isothermal compressibility peaks there observed still serve as an estimate of the state points at which the HDL-LDL correlation is highest. Hence, as a result of the thermodynamic findings, the LDL-like region shrinks upon increasing the concentration as reported in Fig. 9.

4. Structural results

The structural properties of the systems studied can be analysed through the radial distribution functions (RDFs) $g(r)$ [28,6].

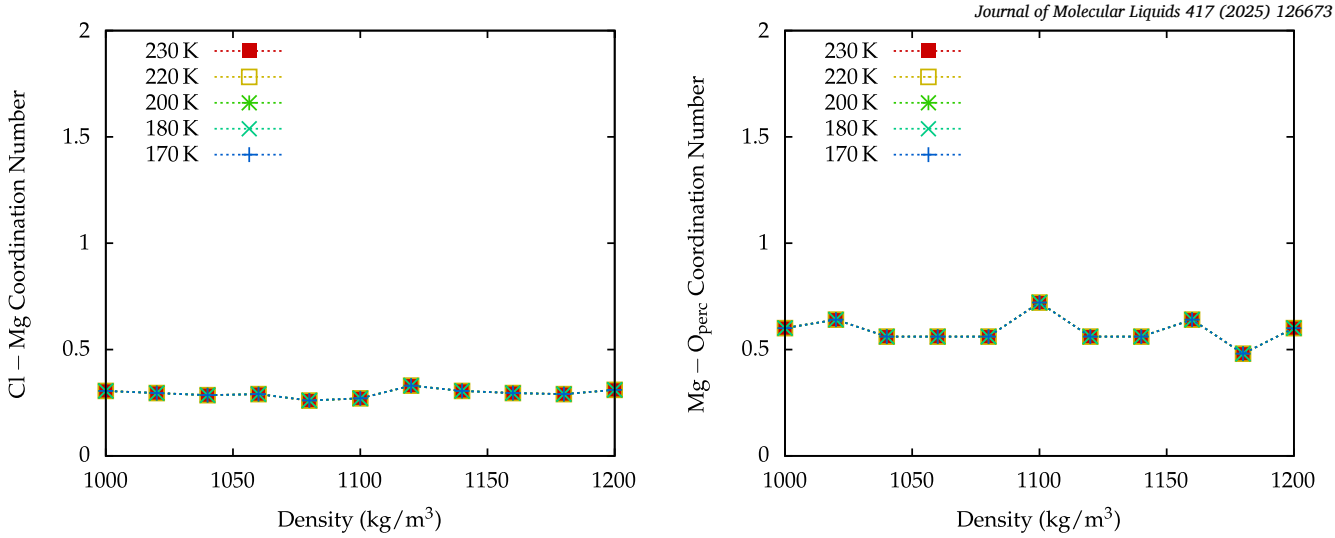

(a) Cl – Mg Coordination Number

(b) Mg – $O_{perchlorate}$ Coordination Number

Fig. 14. Ion-ion first shell coordination numbers for the C_2 solution.

Table 2
Sets of densities to be compared for the $O_W - O_W$ RDFs. The density values were chosen by picking the isochores with similar thermodynamic behaviour at low temperatures.

	ρ_{pure}	ρ_{C_1}	ρ_{C_2} (kg/m^3)
High density triplet	1110	1110	1200
Medium density triplet	990	990	1130
Low density triplet	930	930	1040

The water-water, water-ion and ion-ion RDFs will be considered in the following.

Our analysis is especially focused to understand how LDL and HDL environments are modified in these solutions.

4.1. Water-water RDFs

First, we analyse the water-water RDFs $g_{O_W-O_W}(r)$ for the two solutions and compare them with the corresponding RDFs for pure TIP4P/2005.

As the isochore curves at the same density exhibit markedly different curvatures and a pressure shift upon increasing the concentration, in order to evaluate the structural results we chose to consider for the three systems three sets of densities exhibiting comparable thermodynamic behaviour at low temperatures.

The densities to be compared in triplets are reported in Table 2.

The HDL and the LDL-like structural behaviour of water can be inferred by analysing the water-water (oxygen-oxygen) RDF: relative to the HDL phase, the LDL phase exhibits a deeper first minimum and a sharper second maximum [62–64].

The water-water RDF is reported in Fig. 10 at the three triplets of densities previously defined and at different temperatures.

Down to 300 K, all the solutions under consideration exhibit characteristics typical of the HDL phase. As the temperature further decreases, a shift towards a more LDL-like behaviour gradually occurs.

This behaviour is particularly evident for pure TIP4P/2005 at all investigated densities and it is only slightly less pronounced for the C_1 solution. In fact, apart from the lowest panel in Fig. 10a (at $T = 170\,K, \rho_{pure} = \rho_{C_1} = 1110\,kg/m^3$, where water is very LDL in pure TIP4P/2005), the $g_{O_W-O_W}(r)$ RDF of the C_1 solution closely resembles that of pure TIP4P/2005 at every density and temperature, with minor deviations that can be attributed to slight ion-induced shifts in pressure.

In contrast, the C_2 solution, whilst retaining a trend not dissimilar to that of the other systems, shows a clearer LDL-like behaviour only at low temperatures and low densities.

In Fig. 11 the first shell coordination number is reported for the two solutions.

For both solutions, as densities increase, the coordination numbers show a rising trend. The curves shift downwards as the concentration increases, as more ions are solvated by water molecules.

In the C_1 solution, the coordination among the oxygens of water at lower densities and, particularly, at lower temperatures is typical of LDL water, as inferred by the first-shell O_W-O_W coordination number approaching 4.

At concentration C_2, the tetrahedral structure shows a tendency to distort and therefore the coordination number is not 4. A similar downward shift was observed for other solutions, see for example ref. [38].

4.2. Perchlorate coordination shells

Fig. 12 illustrates the alternating arrangement of ions and water within the C_2 $Mg(ClO_4)_2$-TIP4P/2005 solution around the Cl atom of the perchlorate ion. This is achieved by examining the Cl – H, Cl – Mg, Cl – O_W and Cl – Cl RDFs at high density, $\rho_{C_2} = 1200\,kg/m^3$ (panel (a)), and low density, $\rho_{C_2} = 1040\,kg/m^3$ (panel (b)). Because of the low number of ions in the C_1 solution, only the data for the higher concentration, being statistically more representative, will be presented and discussed.

When considering the Cl-Water RDFs, the perchlorate ion is always surrounded by a cage of water molecules, as H is the first atom to appear, followed in order by the magnesium ion, the oxygen of water, and the chlorine of the perchlorate ion.

Moving on to the Cl – Mg RDFs, we observe that as the temperature falls, there is a significant rise in the first peak of the Cl – Mg ion pairing. This aligns with the observation of reduced ion solubility in the LDL phase, leading to closer proximity between the ions, as observed in Sec. 4.1. Nonetheless, since hydrogen is the first ion present in the coordination shell, we deduce that there is no aggregation. Due to the Coulomb interaction between the two ions, Mg^{2+} and ClO_4^-, only a mild increase in the first peak is observed upon reducing the density. We further observe that the first peak of the Cl-Mg RDFs falls in the solvation shell of water, being in between the first hydrogen and the first oxygen peak.

Relative to the Cl-Cl RDFs, we note that upon lowering the temperature, at sole high density, an increase can be observed for the Cl-Cl

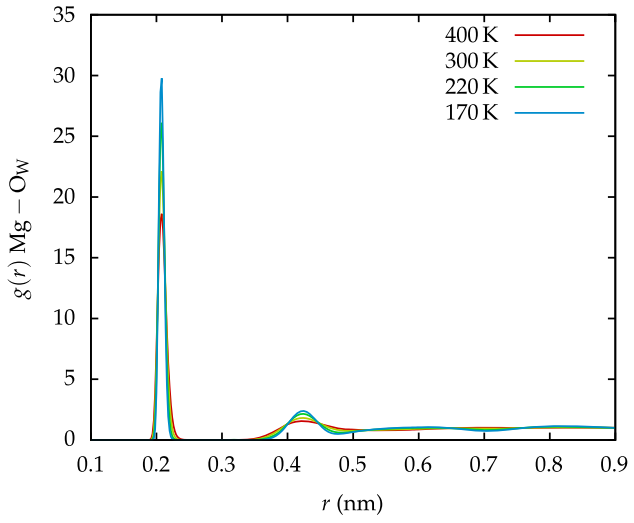

(a) $Mg - O_W$ RDFs at $\rho = 1200\,kg/m^3$

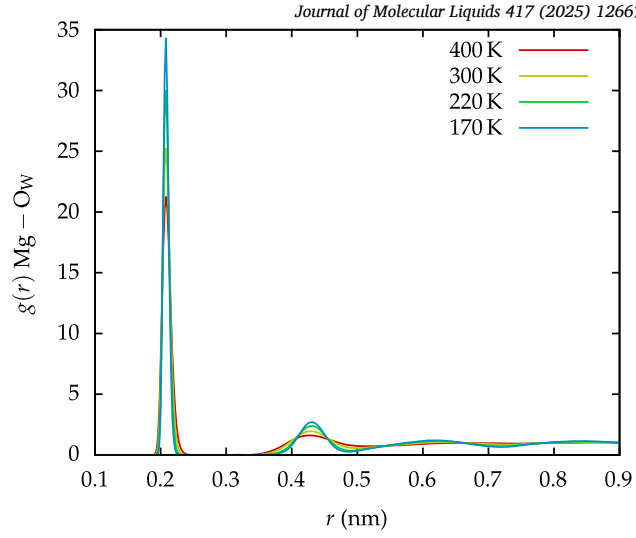

(b) $Mg - O_W$ RDFs at $\rho = 1040\,kg/m^3$

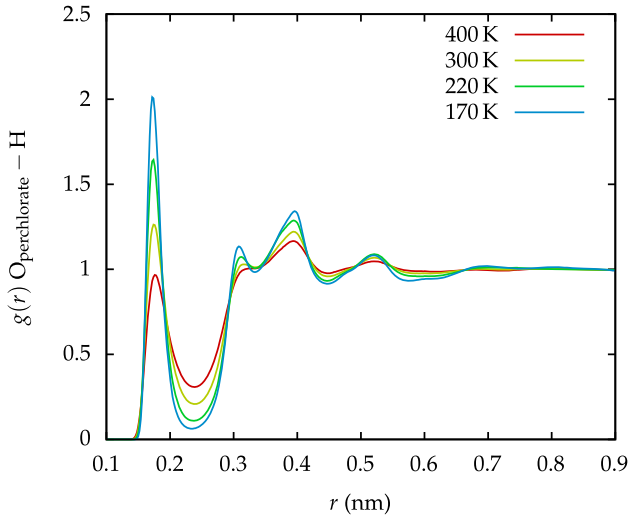

(c) $O_{perchlorate} - H$ RDFs at $\rho = 1200\,kg/m^3$

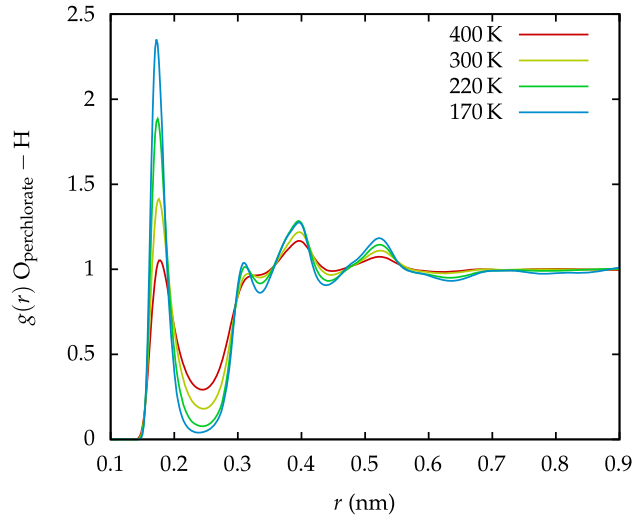

(d) $O_{perchlorate} - H$ RDFs at $\rho = 1040\,kg/m^3$

Fig. 15. Ion-water RDFs for the C_2 solution at densities $\rho = 1200\,kg/m^3$ and $\rho = 1040\,kg/m^3$.

first $g(r)$ peak, which always happens at 0.48 nm. No sign of ordering is observed across the considered ranges of density and temperature.

4.3. Ion pairing

In addition to the Cl-Mg RDFs, which we report again in Fig. 13a and Fig. 13b, we can consider the $Mg - O_{perchlorate}$ ion pairing (Figs. 13c and 13d). As for the previously commented ion pairing, we note that the first peak becomes spikier and more structured particularly with decreasing temperature and to a lesser extent with decreasing density, consistent with the observed tendency of water to exclude ions in LDL which we described in Sec. 4.1.

As further confirmation of the prevalence of the Coulomb interaction with regard to ion pairing, we can observe in Fig. 14 how the ion-ion first shell coordination numbers are substantially unperturbed by density and temperature.

4.4. Ions hydration shells

In Fig. 15 we report the $Mg{-}O_W$ and the $O_{perchlorate} - H$ RDFs which, together with the $Cl - H$ and the $Cl - O_W$ RDFs, can be used to describe the ion-water structural behaviour.

By analysing the first coordination shell of the perchlorate ion (Fig. 12), it was observed that the Mg ion is located within the solvation shell of the Cl.

The reverse is not true, as the first solvation shell of the Mg is positioned at the first minimum of the $g_{Mg-O_W}(r)$ (Figs. 15a and 15b) at around 0.21 nm, while the $g_{Cl-Mg}(r)$ remains close to zero at 0.3 nm (Figs. 13a and 13b). This phenomenon is also computationally observed in $NaClO_4$ [65,40].

The first peaks of the $g_{O_{perchlorate}-H}(r)$ suggest the presence of structured hydrogen bonds between the anion and water. The height of the first peak increases as the temperature decreases, indicating that hydrogen bonds are stronger and more persistent at lower temperatures. As T increases, the greater thermal mobility results in decreased first peaks.

4.5. Ion-water coordination numbers

Fig. 16 shows the ion-water first shell coordination numbers for the C_2 solution.

The $Cl - O_W$ coordination number (Fig. 16a) exhibits a similar trend in density and temperature to that observed for $O_W - O_W$ (Fig. 11). Upon reducing the volume of the system, the $Cl{-}O_W$ RDF first minimum becomes less structured, until it disappears at high density (see Figs. 12 and

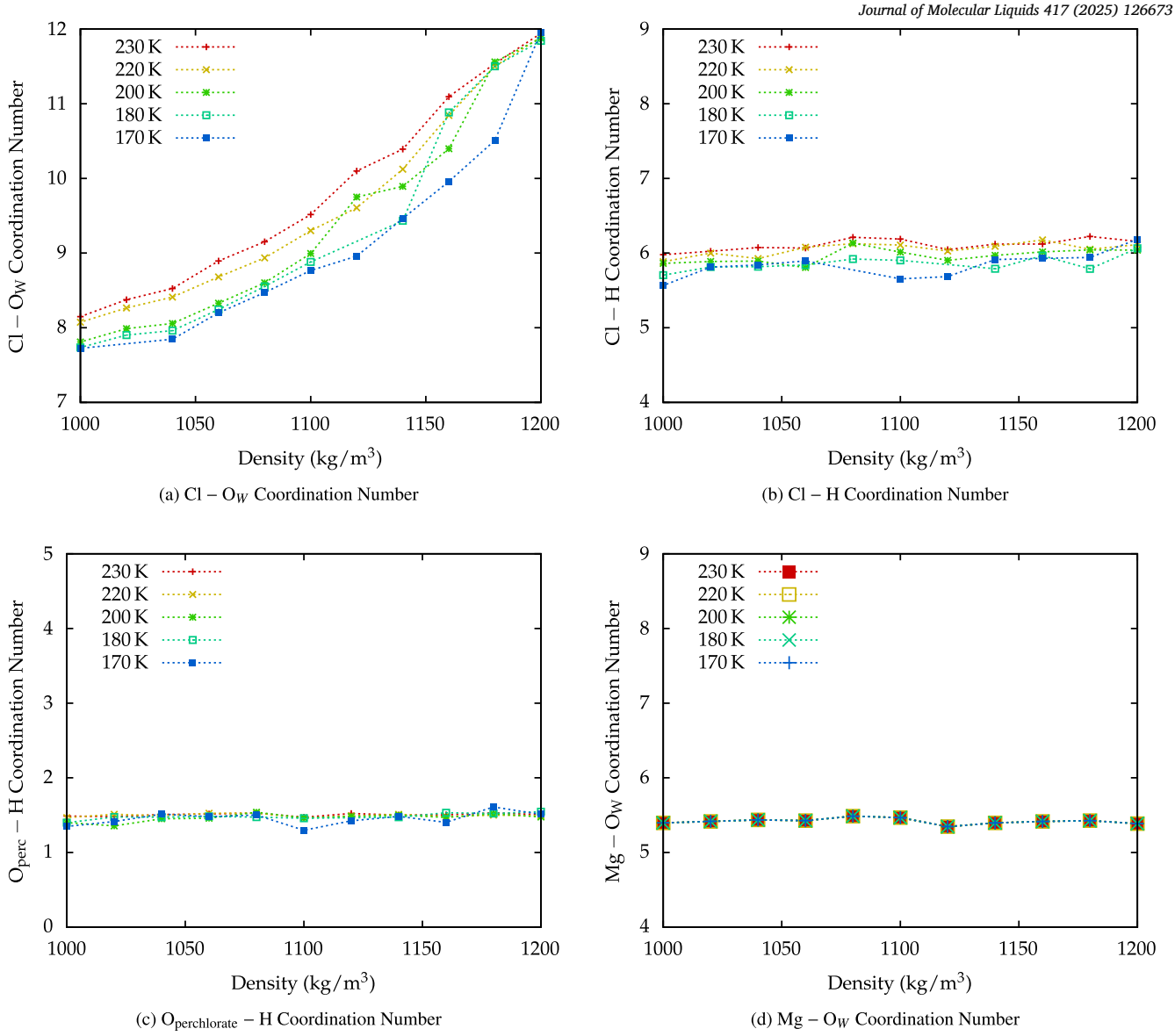

(a) Cl – O_W Coordination Number

(b) Cl – H Coordination Number

(c) $O_{perchlorate}$ – H Coordination Number

(d) Mg – O_W Coordination Number

Fig. 16. Ion-water coordination numbers for the C_2 solution.

17a). In order to compute the number of first neighbours, we chose to use a fixed 0.43 nm radius to compute the Cl – O_W coordination number.

The Cl – H (Fig. 16b) coordination numbers are slightly lower than those for Cl – O_W, due to the greater peak heights in the $g(r)_{Cl-O_W}$ (Fig. 12) and the wider Cl – O_W first shell. The Cl–H RDF always exhibits a well structured first minimum at about 0.34 nm (Fig. 17b), at variance with the Cl–O_W. Furthermore, concerning the Cl – H coordination, there appears to be a statistical trend indicating an increase in the coordination number with temperature, attributed to higher thermal mobility upon increasing the temperature, while the number remains essentially unchanged with increasing density. This last phenomenon is related with the ion pairing coordination numbers of Fig. 14. In fact, when we look at the alternation of ions around the perchlorate, Fig. 12, we see that the positive charges closer to the perchlorates are both hydrogens and magnesium ions, the hydrogen being closer. The strength of the ion-pairing between the ions appears to trap the hydrogen in a shell that does not change when density changes. Related to what just observed we find that essentially constant across temperatures and densities are also the $O_{perchlorate}$ – H (Fig. 16c) coordination numbers.

The Mg – O_W (Fig. 16d) first shell coordination numbers are substantially unaffected by changes in temperature and density. This is likely related to the fact that the stronger Coulomb interactions of the Mg overshadow the influence of thermal and density fluctuations.

5. Comparison with $NaClO_4$

A similar study on aqueous solutions of sodium perchlorate ($NaClO_4$) was performed in [40], with concentrations ${C_1}^{NaClO_4} = 1.63\,wt\%$ and ${C_2}^{NaClO_4} = 15.4\,wt\%$. In mole fractions, the two concentrations are ${C_1}^{NaClO_4} = 2.43 \times 10^{-3}$ (similar to the ${C_1}^{Mg(ClO_4)_2}$ solution) and ${C_2}^{NaClO_4} = 26.1 \times 10^{-3}$ (similar to the ${C_2}^{Mg(ClO_4)_2}$ solution).

Sodium perchlorate is among the salts known to be present on Mars, although the role of magnesium perchlorate in the presence of liquid water on Mars could be more relevant than that of sodium perchlorate [41,42].

A comparable number of water molecules was considered in the four systems, but while the ${C_1}^{NaClO_4}$ solution contains 20 ions (10 sodium, 10 perchlorates), the ${C_1}^{Mg(ClO_4)_2}$ solution contains 30 ions (10 magnesium, 20 perchlorates). Likewise, the ${C_2}^{NaClO_4}$ solution contains 200 ions, while the ${C_2}^{Mg(ClO_4)_2}$ solution contains 300 ions.

The persistence of several thermodynamic and structural water anomalies reported in this study was also observed in [40]. In addition to the downward shift in temperature, the TMD and the TmD curves

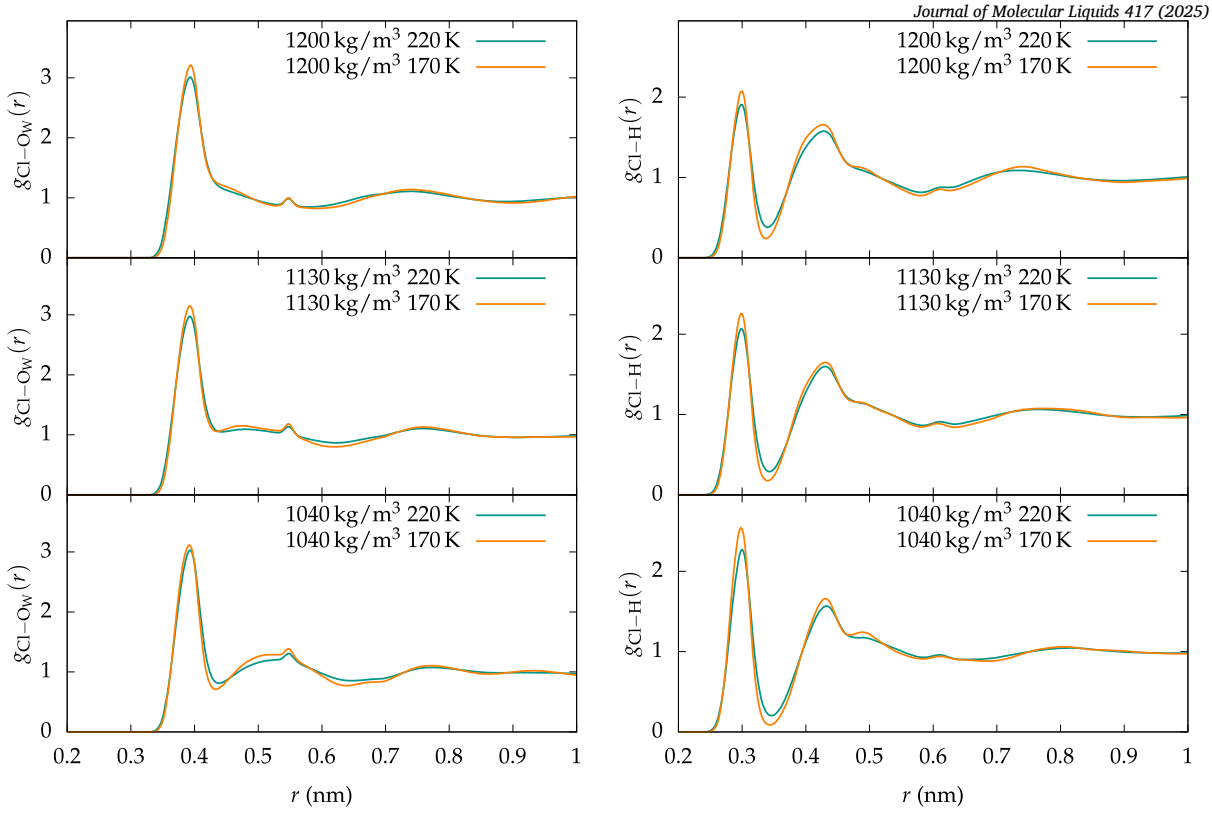

(a) Cl − O_W RDF

(b) Cl − H RDF

Fig. 17. Cl−O_W and Cl−H radial distribution functions.

were observed shifting to lower pressures, maxima in κ_T were also observed, as well as an LG-LMS substantially unchanged in position.

A liquid-liquid critical point was observed in the ${C_1}^{NaClO_4}$ and in the ${C_2}^{NaClO_4}$ solutions in [40], and only in the ${C_1}^{Mg(ClO_4)_2}$ solution in this paper. We observe that upon increasing the $NaClO_4$ concentration, the LLCP was observed shifting to higher temperatures and lower pressures.

From a structural point of view, a shift from an HDL-like to an LDL-like behaviour was observed across the four solutions. Apart from slight differences at high densities and low temperatures, the ${C_1}^{NaClO_4}$ solution, like the ${C_1}^{Mg(ClO_4)_2}$ one, behaved essentially the same as pure TIP4P/2005. An increase in the first peak of the ion pairing was observed for the $NaClO_4$ solutions both upon lowering the temperatures (as for the $Mg(ClO_4)_2$) solutions) and the densities (unlike the $Mg(ClO_4)_2$) solutions). The difference in the behaviour is explained by the higher Coulomb interaction between the magnesium and the perchlorate ions.

Unlike the current study, the chlorine ions were observed ordering for the ${C_2}^{NaClO_4}$ solution at low density and low temperatures, therefore implying a more stabilised supercooled region of water for aqueous solutions of magnesium perchlorate.

6. Conclusions

Given the growing interest in perchlorate aqueous solutions, driven by recent experimental evidence on the presence of supercooled liquid water in these solutions beneath the Martian soil [41,42], it was crucial to investigate their thermodynamic and structural features and the role of water anomalies in this context.

A concentration-dependent thermodynamic and structural study of aqueous solutions of magnesium perchlorate based on MD simulations [6,28] was carried out in the canonical ensemble. Two concentrations were considered, 2.95 wt% (mole fraction 2.45×10^{-3}) and 24.4 wt% (mole fraction 25.4×10^{-3}).

The phase diagram analysis highlighted the persistence of several water anomalies. The hypothesised LLCP [8] was found to be present at a low concentration of the solute, although with a minor shift in pressure, while the temperature was substantially the same.

A shift towards lower temperatures was observed for the TMD and the TmD curves. No evidence of LLCP was found in the C_2 solution.

A significant anomaly shared with pure water, observed in all solutions, was the occurrence of maxima in the isothermal compressibility. This finding holds considerable weight as lines of maxima in thermodynamic response functions near the LLCP (and, generally speaking, near second-order critical points) tend to converge towards the Widom Line. The Widom Line serves as a precursor to the LLCP, converging to it before extending into the two-phase region as the HDL-LDL coexistence line, in the case of supercooled water.

The existence of a line of maxima for isothermal compressibility for the C_2 solution, characterised by increasingly prominent peaks as the temperature decreases towards the lowest achievable equilibration point with MD, does not exclude the potential presence of a second-order critical point at lower temperatures.

The state points corresponding to the isothermal compressibility maxima were observed shifting to lower pressures upon increasing the concentration of the solutes. The LG-LMS curve, on the other hand, was observed to be substantially unaltered in pressure by the solutes.

Therefore, we noted a contraction of the LDL region of water, where nucleation is more likely [1], as the concentration of the solute is increased. Hence, as the concentration is increased, the supercooled phase extends its region of existence.

The persistence of water anomalies is further corroborated by the water-water, water-ion, and ion-ion radial distribution functions (RDFs). Notably, ion pairing was found to be favoured by a reduction in temperature. Such behaviour typically occurs in the LDL region, whereas in HDL water the ions tend to be more favourably solvated.

The water-water RDFs also revealed an interplay between the HDL and LDL phases of water, with water exhibiting a less LDL-like behaviour upon increasing the concentration.

Similar to pure TIP4P/2005, the water-water RDFs exhibited a shift from HDL to LDL behaviour at lower densities and temperatures. Interestingly, at high concentrations, LDL features only emerged at very low temperatures and densities, and were less pronounced than in pure water.

Further evidence for a more extended region of existence of the supercooled water phase comes from the analysis of Cl-Cl RDFs in the magnesium perchlorate solution. At low densities and temperatures, these functions do not exhibit ordered structures.

In light of recent discoveries regarding the presence of liquid water on Mars, our results have shown that water can retain its anomalous properties even when mixed with magnesium perchlorate, a typical Martian salt. These anomalies could be a key factor in explaining the existence of supercooled liquid water on Mars. In particular, the LLCP issue and the related thermodynamic lines, like the Widom line, are most important to assess the tendency of water to avoid crystallisation in solutions. The prevalence of HDL helps water to remain liquid.

CRediT authorship contribution statement

Paolo La Francesca: Writing – review & editing, Writing – original draft, Investigation, Data curation. **Paola Gallo:** Writing – review & editing, Writing – original draft, Supervision, Investigation, Funding acquisition, Resources, Data curation, Conceptualization, Validation, Project administration.

Declaration of competing interest

The authors declare that they have no known competing financial interests or personal relationships that could have appeared to influence the work reported in this paper.

Acknowledgements

The research was supported by PNRR-M4C2-I1.1-PRIN 2022-PE9-ARES - Assessing the origin and stability of Martian subglacial waters - F53D23001240006 - Funded by EU - NextGenerationEU.

Data availability

Data will be made available on request.

References

[1] P. Gallo, K. Amann-Winkel, C.A. Angell, M.A. Anisimov, F. Caupin, C. Chakravarty, E. Lascaris, T. Loerting, A.Z. Panagiotopoulos, J. Russo, J.A. Sellberg, H.E. Stanley, H. Tanaka, C. Vega, L. Xu, L.G.M. Pettersson, Water: a tale of two liquids, Chem. Rev. 116 (13) (2016) 7463–7500, https://doi.org/10.1021/acs.chemrev.5b00750.

[2] P. Gallo, H.E. Stanley, Supercooled water reveals its secrets, Science 358 (6370) (2017) 1543–1544, https://doi.org/10.1126/science.aar3575, https://www.science.org/doi/pdf/10.1126/science.aar3575, https://www.science.org/doi/abs/10.1126/science.aar3575.

[3] P.G. Debenedetti, Supercooled and glassy water, J. Phys. Condens. Matter 15 (45) (2003) R1669–R1726, https://doi.org/10.1088/0953-8984/15/45/r01.

[4] C.A. Angell, Supercooled water, Annu. Rev. Phys. Chem. 34 (1) (1983) 593–630, https://doi.org/10.1146/annurev.pc.34.100183.003113.

[5] P. Debenedetti, Metastable Liquids: Concepts and Principles, Physical Chemistry: Science and Engineering, Princeton University Press, 1996, https://books.google.it/books?id=tzvvsltE6Y8C.

[6] P. Gallo, M. Rovere, Physics of Liquid Matter, Soft and Biological Matter, Springer International Publishing, 2021, https://books.google.it/books?id=aT83EAAAQBAJ.

[7] F.H. Stillinger, A. Rahman, Improved simulation of liquid water by molecular dynamics, J. Chem. Phys. 60 (4) (1974) 1545–1557, https://doi.org/10.1063/1.1681229.

[8] P.H. Poole, F. Sciortino, U. Essmann, H.E. Stanley, Phase behaviour of metastable water, Nature 360 (1992) 324–328, https://doi.org/10.1038/360324a0.

[9] J.C. Palmer, F. Martelli, Y. Liu, R. Car, A.Z. Panagiotopoulos, P.G. Debenedetti, Metastable liquid–liquid transition in a molecular model of water, Nature 510 (7505) (2014) 385–388, https://doi.org/10.1038/nature13405.

[10] Y. Liu, J.C. Palmer, A.Z. Panagiotopoulos, P.G. Debenedetti, Liquid-liquid transition in st2 water, J. Chem. Phys. 137 (21) (2012) 214505, https://doi.org/10.1063/1.4769126.

[11] Y. Liu, A.Z. Panagiotopoulos, P.G. Debenedetti, Low-temperature fluid-phase behavior of st2 water, J. Chem. Phys. 131 (10) (2009) 104508, https://doi.org/10.1063/1.3229892.

[12] F. Sciortino, I. Saika-Voivod, P.H. Poole, Study of the st2 model of water close to the liquid–liquid critical point, Phys. Chem. Chem. Phys. 13 (2011) 19759–19764, https://doi.org/10.1039/C1CP22316J.

[13] T.A. Kesselring, E. Lascaris, G. Franzese, S.V. Buldyrev, H.J. Herrmann, H.E. Stanley, Finite-size scaling investigation of the liquid-liquid critical point in st2 water and its stability with respect to crystallization, J. Chem. Phys. 138 (24) (2013) 244506, https://doi.org/10.1063/1.4808355.

[14] F. Smallenburg, F. Sciortino, Tuning the liquid-liquid transition by modulating the hydrogen-bond angular flexibility in a model for water, Phys. Rev. Lett. 115 (2015) 015701, https://doi.org/10.1103/PhysRevLett.115.015701, https://link.aps.org/doi/10.1103/PhysRevLett.115.015701.

[15] E.A. Jagla, Low-temperature behavior of core-softened models: water and silica behavior, Phys. Rev. E 63 (2001) 061509, https://doi.org/10.1103/PhysRevE.63.061509, https://link.aps.org/doi/10.1103/PhysRevE.63.061509.

[16] P. Gallo, F. Sciortino, Ising universality class for the liquid-liquid critical point of a one component fluid: a finite-size scaling test, Phys. Rev. Lett. 109 (17) (2012) 177801, https://doi.org/10.1103/PhysRevLett.109.177801.

[17] J.L. Abascal, C. Vega, A general purpose model for the condensed phases of water: Tip4p/2005, J. Chem. Phys. 123 (23) (2005) 234505, https://doi.org/10.1063/1.2121687.

[18] J.L.F. Abascal, E. Sanz, R. García Fernández, C. Vega, A potential model for the study of ices and amorphous water: TIP4P/Ice, J. Chem. Phys. 122 (23) (2005) 234511, https://doi.org/10.1063/1.1931662, https://pubs.aip.org/aip/jcp/article-pdf/doi/10.1063/1.1931662/13134473/234511_1_online.pdf.

[19] P.G. Debenedetti, F. Sciortino, G.H. Zerze, Second critical point in two realistic models of water, Science 369 (6501) (2020) 289–292, https://doi.org/10.1126/science.abb9796, https://www.science.org/doi/pdf/10.1126/science.abb9796, https://www.science.org/doi/abs/10.1126/science.abb9796.

[20] O. Mishima, H.E. Stanley, Decompression-induced melting of ice iv and the liquid–liquid transition in water, Nature 392 (6672) (1998) 164–168, https://doi.org/10.1038/32386.

[21] K.H. Kim, A. Späh, H. Pathak, F. Perakis, D. Mariedahl, K. Amann-Winkel, J.A. Sellberg, J.H. Lee, S. Kim, J. Park, et al., Maxima in the thermodynamic response and correlation functions of deeply supercooled water, Science 358 (6370) (2017) 1589–1593, https://doi.org/10.1126/science.aap826.

[22] S. Woutersen, B. Ensing, M. Hilbers, Z. Zhao, C.A. Angell, A liquid-liquid transition in supercooled aqueous solution related to the hda-lda transition, Science 359 (6380) (2018) 1127–1131, https://doi.org/10.1126/science.aao7049.

[23] K.H. Kim, K. Amann-Winkel, N. Giovambattista, A. Späh, F. Perakis, H. Pathak, M.L. Parada, C. Yang, D. Mariedahl, T. Eklund, T.J. Lane, S. You, S. Jeong, M. Weston, J.H. Lee, I. Eom, M. Kim, J. Park, S.H. Chun, P.H. Poole, A. Nilsson, Experimental observation of the liquid-liquid transition in bulk supercooled water under pressure, Science 370 (6519) (2020) 978–982, https://doi.org/10.1126/science.abb9385, https://www.science.org/doi/pdf/10.1126/science.abb9385, https://www.science.org/doi/abs/10.1126/science.abb9385.

[24] K. Winkel, E. Mayer, T. Loerting, Equilibrated high-density amorphous ice and its first-order transition to the low-density form, J. Phys. Chem. B 115 (48) (2011) 14141–14148, https://doi.org/10.1021/jp203985w.

[25] R.J. Speedy, P.G. Debenedetti, R.S. Smith, C. Huang, B.D. Kay, The evaporation rate, free energy, and entropy of amorphous water at 150 k, J. Chem. Phys. 105 (1) (1996) 240–244, https://doi.org/10.1063/1.471869.

[26] A. Nilsson, Origin of the anomalous properties in supercooled water based on experimental probing inside “no-man’s land”, J. Non-Cryst. Solids X 14 (2022) 100095, https://doi.org/10.1016/j.nocx.2022.100095.

[27] M. Seidl, A. Fayter, J.N. Stern, G. Zifferer, T. Loerting, Shrinking water’s no man’s land by lifting its low-temperature boundary, Phys. Rev. B 91 (2015) 144201, https://doi.org/10.1103/PhysRevB.91.144201, https://link.aps.org/doi/10.1103/PhysRevB.91.144201.

[28] M. Allen, D. Tildesley, D. Tildesley, Computer Simulation of Liquids, Oxford science publications, Oxford University Press, 2017, https://books.google.it/books?id=nlExDwAAQBAJ.

[29] L. Xu, P. Kumar, S.V. Buldyrev, S.-H. Chen, P.H. Poole, F. Sciortino, H.E. Stanley, Relation between the Widom line and the dynamic crossover in systems with a liquid–liquid phase transition, Proc. Natl. Acad. Sci. 102 (46) (2005) 16558–16562, https://doi.org/10.1073/pnas.0507870102.

[30] G. Franzese, H.E. Stanley, The Widom line of supercooled water, J. Phys. Condens. Matter 19 (20) (2007) 205126, https://doi.org/10.1088/0953-8984/19/20/205126.

[31] J.L. Abascal, C. Vega, Widom line and the liquid–liquid critical point for the tip4p/2005 water model, J. Chem. Phys. 133 (23) (2010) 234502, https://doi.org/10.1063/1.3506860.

[32] P. Gallo, M. Rovere, Mode coupling and fragile to strong transition in supercooled tip4p water, J. Chem. Phys. 137 (16) (2012) 164503, https://doi.org/10.1063/1.4759262.

[33] M. De Marzio, G. Camisasca, M. Rovere, P. Gallo, Mode coupling theory and fragile to strong transition in supercooled tip4p/2005 water, J. Chem. Phys. 144 (7) (2016) 074503, https://doi.org/10.1063/1.4941946.

[34] L. Lupi, B. Vázquez Ramírez, P. Gallo, Dynamical crossover and its connection to the Widom line in supercooled tip4p/ice water, J. Chem. Phys. 155 (5) (2021) 054502, https://doi.org/10.1063/5.0059190.

[35] P. Gallo, D. Corradini, M. Rovere, Widom line and dynamical crossovers as routes to understand supercritical water, Nat. Commun. 5 (1) (2014) 5806, https://doi.org/10.1038/ncomms6806.

[36] D.G. Archer, R.W. Carter, Thermodynamic properties of the nacl + h2o system. 4. Heat capacities of h2o and nacl(aq) in cold-stable and supercooled states, J. Phys. Chem. B 104 (35) (2000) 8563–8584, https://doi.org/10.1021/jp0003914.

[37] D. Corradini, M. Rovere, P. Gallo, A route to explain water anomalies from results on an aqueous solution of salt, J. Chem. Phys. 132 (2010) 134508, https://doi.org/10.1063/1.3376776.

[38] D. Corradini, Z. Su, H.E. Stanley, P. Gallo, A molecular dynamics study of the equation of state and the structure of supercooled aqueous solutions of methanol, J. Chem. Phys. 137 (18) (2012) 184503, https://doi.org/10.1063/1.4767060.

[39] L. Perin, P. Gallo, Phase diagram of aqueous solutions of licl: a study of concentration effects on the anomalies of water, J. Phys. Chem. B 127 (20) (2023) 37167579, https://doi.org/10.1021/acs.jpcb.3c00703.

[40] P. La Francesca, P. Gallo, Supercooled solutions of sodium perchlorate in TIP4P/2005 water: the effect of martian solutes on thermodynamics and structure, J. Chem. Phys. 159 (12) (2023) 124501, https://doi.org/10.1063/5.0168587, https://pubs.aip.org/aip/jcp/article-pdf/doi/10.1063/5.0168587/18136708/124501_1_5.0168587.pdf.

[41] R. Orosei, S.E. Lauro, E. Pettinelli, A. Cicchetti, M. Coradini, B. Cosciotti, F.D. Paolo, E. Flamini, E. Mattei, M. Pajola, F. Soldovieri, M. Cartacci, F. Cassenti, A. Frigeri, S. Giuppi, R. Martufi, A. Masdea, G. Mitri, C. Nenna, R. Noschese, M. Restano, R. Seu, Radar evidence of subglacial liquid water on Mars, Science 361 (6401) (2018) 490–493, https://doi.org/10.1126/science.aar7268, https://www.science.org/doi/pdf/10.1126/science.aar7268, https://www.science.org/doi/abs/10.1126/science.aar7268.

[42] S.E. Lauro, E. Pettinelli, G. Caprarelli, L. Guallini, A.P. Rossi, E. Mattei, B. Cosciotti, A. Cicchetti, F. Soldovieri, M. Cartacci, F. Di Paolo, R. Noschese, R. Orosei, Multiple subglacial water bodies below the south pole of Mars unveiled by new marsis data, Nat. Astron. 5 (2021) 63–70, https://doi.org/10.1038/s41550-020-1200-6.

[43] J. Toner, D. Catling, B. Light, The formation of supercooled brines, viscous liquids, and low-temperature perchlorate glasses in aqueous solutions relevant to Mars, Icarus 233 (2014) 36–47, https://doi.org/10.1016/j.icarus.2014.01.018.

[44] S. Lenton, N.H. Rhys, J.J. Towey, A.K. Soper, L. Dougan, Highly compressed water structure observed in a perchlorate aqueous solution, Nat. Commun. 8 (1) (October 2017), https://doi.org/10.1038/s41467-017-01039-9.

[45] H. Laurent, A. Soper, L. Dougan, Biomolecular self-assembly under extreme martian mimetic conditions, Mol. Phys. 117 (22) (2019) 3398–3407, https://doi.org/10.1080/00268976.2019.1649485.

[46] H. Laurent, A.K. Soper, L. Dougan, Trimethylamine n-oxide (tmao) resists the compression of water structure by magnesium perchlorate: terrestrial kosmotrope vs. martian chaotrope, Phys. Chem. Chem. Phys. 22 (2020) 4924–4937, https://doi.org/10.1039/C9CP06324B.

[47] C. Calvagna, A. Lapini, A. Taschin, S. Fanetti, M. Pagliai, P. Bartolini, R. Bini, R. Righini, R. Torre, Modification of local and collective dynamics of water in perchlorate solution, induced by pressure and concentration, J. Mol. Liq. 337 (2021) 116273, https://doi.org/10.1016/j.molliq.2021.116273, https://www.sciencedirect.com/science/article/pii/S0167732221009971.

[48] W. Humphrey, A. Dalke, K. Schulten, Vmd: visual molecular dynamics, J. Mol. Graph. 14 (1) (1996) 33–38, https://doi.org/10.1016/0263-7855(96)00018-5.

[49] H. Bekker, H. Berendsen, E. Dijkstra, S. Achterop, R. Vondrumen, D. Vanderspoel, A. Sijbers, H. Keegstra, M. Renardus, Gromacs-a parallel computer for molecular-dynamics simulations, in: 4th International Conference on Computational Physics (PC 92), World Scientific Publishing, 1993, pp. 252–256.

[50] H.J. Berendsen, D. van der Spoel, R. van Drunen, Gromacs: a message-passing parallel molecular dynamics implementation, Comput. Phys. Commun. 91 (1–3) (1995) 43–56, https://doi.org/10.1016/0010-4655(95)00042-e.

[51] B. Hess, C. Kutzner, D. van der Spoel, E. Lindahl, Gromacs 4: algorithms for highly efficient, load-balanced, and scalable molecular simulation, J. Chem. Theory Comput. 4 (3) (2008) 435–447, https://doi.org/10.1021/ct700301q.

[52] V.N. Agieienko, Y.V. Kolesnik, O.N. Kalugin, Structure, solvation, and dynamics of Mg2+, Ca2+, Sr2+, and Ba2+ complexes with 3-hydroxyflavone and perchlorate anion in acetonitrile medium: a molecular dynamics simulation study, J. Chem. Phys. 140 (19) (2014) 194501, https://doi.org/10.1063/1.4875591, https://pubs.aip.org/aip/jcp/article-pdf/doi/10.1063/1.4875591/9543311/194501_1_online.pdf.

[53] J. Åqvist, Ion-water interaction potentials derived from free energy perturbation simulations, J. Phys. Chem. 94 (21) (1990) 8021–8024, https://doi.org/10.1021/j100384a009.

[54] G. Heinje, W.A.P. Luck, K. Heinzinger, Molecular dynamics simulation of an aqueous sodium perchlorate solution, J. Phys. Chem. 91 (2) (1987) 331–338, https://doi.org/10.1021/j100286a020.

[55] U. Essmann, L. Perera, M.L. Berkowitz, T. Darden, H. Lee, L.G. Pedersen, A smooth particle mesh Ewald method, J. Chem. Phys. 103 (19) (1995) 8577–8593, https://doi.org/10.1063/1.470117.

[56] G. Bussi, D. Donadio, M. Parrinello, Canonical sampling through velocity rescaling, J. Chem. Phys. 126 (1) (2007) 014101, https://doi.org/10.1063/1.2408420.

[57] E. Lascaris, The effect of intra-molecular bonds on the liquid–liquid critical point in modified-wac models, J. Chem. Phys. 157 (20) (2022) 204501, https://doi.org/10.1063/5.0123159.

[58] D. Liu, Y. Zhang, C.-C. Chen, C.-Y. Mou, P.H. Poole, S.-H. Chen, Observation of the density minimum in deeply supercooled confined water, Proc. Natl. Acad. Sci. 104 (23) (2007) 9570–9574, https://doi.org/10.1073/pnas.0701352104.

[59] D. Paschek, How the liquid-liquid transition affects hydrophobic hydration in deeply supercooled water, Phys. Rev. Lett. 94 (21) (June 2005), https://doi.org/10.1103/physrevlett.94.217802.

[60] P.H. Poole, I. Saika-Voivod, F. Sciortino, Density minimum and liquid–liquid phase transition, J. Phys. Condens. Matter 17 (43) (2005) L431–L437, https://doi.org/10.1088/0953-8984/17/43/l01.

[61] J.W. Biddle, R.S. Singh, E.M. Sparano, F. Ricci, M.A. González, C. Valeriani, J.L.F. Abascal, P.G. Debenedetti, M.A. Anisimov, F. Caupin, Two-structure thermodynamics for the tip4p/2005 model of water covering supercooled and deeply stretched regions, J. Chem. Phys. 146 (3) (2017) 034502, https://doi.org/10.1063/1.4973546.

[62] A.K. Soper, M.A. Ricci, Structures of high-density and low-density water, Phys. Rev. Lett. 84 (13) (2000) 2881–2884, https://doi.org/10.1103/physrevlett.84.2881.

[63] D. Corradini, M. Rovere, P. Gallo, Structural properties of high and low density water in a supercooled aqueous solution of salt, J. Phys. Chem. B 115 (6) (2011) 1461–1468, https://doi.org/10.1021/jp1101237.

[64] P. Gallo, D. Corradini, M. Rovere, Ion hydration and structural properties of water in aqueous solutions at normal and supercooled conditions: a test of the structure making and breaking concept, Phys. Chem. Chem. Phys. 13 (44) (2011) 19814–19822, https://doi.org/10.1039/C1CP22166C.

[65] I.J. General, E.K. Asciutto, J.D. Madura, Structure of aqueous sodium perchlorate solutions, J. Phys. Chem. B 112 (48) (2008) 15417–15425, https://doi.org/10.1021/jp806269w.